Recognition and catalytic mechanism of tRNA m^3C methyltransferase METTL6

Jana Aupič[1], Alessandra Magistrato[1,*]

[1]CNR - Istituto Officina dei Materiali (IOM), Trieste, Italy

[*]Corresponding author email: alema@sissa.it

Abstract

Post-transcriptional RNA modifications importantly impact RNA structural and functional landscape, and thus play a central role in many cellular processes. Accordingly, aberrant RNA modification pathways underpin a variety of human diseases, including cancer and neurological disorders. However, recognition and catalytic mechanisms of RNA modifying proteins remain obfuscate, due to sparce structural data. Recently, cryogenic electron microscopy structure of m^3C methyltransferase METTL6 in complex with $tRNA^{Ser}$ and seryl-tRNA synthetase (SerRS) was reported. Here, we employ multi-scale computer simulations to ascertain how METTL6, assisted by SerRS, identifies its $tRNA^{Ser}$ substrate and catalyzes m^3C_{32} formation. We demonstrate SerRS acts by engaging $tRNA^{Ser}$ variable arm to create the interaction surface for METTL6 recruitment. Once METTL6 is appropriately docked at the $tRNA^{Ser}$ anticodon stem loop, the methylation reaction proceeds spontaneously. These findings establish the catalytic mechanism of m^3C RNA methyltransferases and suggest promising avenues for therapeutic targeting.

Introduction

RNA molecules possess remarkable structural and functional diversity, rivalling that of proteins. While composed of only four nucleotides, the chemical richness of RNA is greatly enhanced by post-transcriptional modifications with more than 170 modifications uncovered so far. Methylation is decidedly the most frequent modification and its deposition is catalysed by a diverse group of enzymes, termed RNA methyltransferase proteins (RMPs). As RNA modifications influence stability, folding, structure and function of RNA molecules, and how they form larger multicomponent assemblies, they are important regulators of gene expression(*1–3*). This is particularly evident in case of tRNA molecules, where RNA covalent modifications affect their function as mRNA decoders in protein synthesis (*4*). Modifications in the anticodon stem loop were shown to directly affect tRNA-mRNA codon interactions and thus influence translation fidelity (i.e. correct reading of the codon sequence) and translation rate(*4–6*). Instead, modifications outside of the anticodon stem loop regulate mRNA translation by modulating tRNA folding, which can affect its interactions with the appropriate aminoacyl-tRNA synthetase and/or the ribosome, and tRNA stability, which is reflected in tRNA abundance(*4*). Thus, deposition or removal of tRNA modifications can lead to preferential translation of mRNA transcripts with high content of certain codons(*7*). Interestingly, several lines of evidence suggest that this so-called codon-biased translation is an important mechanism of cellular response to changing environmental factors, such as high oxidative stress, and is also employed by cancer cells for proteome reprogramming to drive cancer cell phenotypes, such as cell proliferation, metastasis and cell survival(*4*, *7*, *8*). Indeed, among RNA classes tRNA molecules are most affected by RNA modification.

Hitherto, a plethora of diverse RMPs targeting tRNAs (tRMPs) have been discovered and linked to specific modifications(*3*, *9*, *10*). However, due to inherent flexibility of RNA, and tRNA by extension, detailed high-resolution structural characterization of tRMPs in complex with their target tRNA is challenging. Indeed, only a handful of tRMP-tRNA structures have been resolved so far(*11–13*), limiting our understanding of tRMPs recognition and catalytic mechanisms. This in turn is preventing the comprehensive assessment of tRMPs as novel anticancer targets and identification of viable drug targeting strategies. Recently, Eva Kowalinski and colleagues have reported the structure of a 3-methylcytidine (m^3C) methyltransferase METTL6 in complex with its tRNA substrate with cryogenic electron microscopy (cryo-EM)(*11*).

METTL6 is a highly specific enzyme, responsible for the formation of m^3C at position 32 in the anticodon stem loop of $tRNA^{Ser}$(*14*). It utilizes S-adenosyl-L-methionine (SAM) substrate as the source of the methyl group and needs seryl-tRNA synthetase (SerRS) for $tRNA^{Ser}$ binding and recognition(*15*). SerRS was proposed to rearrange the $tRNA^{Ser}$ anticodon stem loop for optimal METTL6 binding, however the exact mechanism is unclear(*16*). As observed for several tRNA methyltransferases, METTL6 expression is deregulated in multiple cancer types, including pancreatic, breast and liver cancer(*17–19*). Knockout of METTL6 in mouse embryonic stem cells reduced liver cancer cell proliferation and impaired colony formation capacity, suggesting it is a viable anticancer target(*17–19*). Furthermore, breast cancer cells lacking METTL6 showed greater sensitivity to cisplatin(*20*). Other representatives of the m^3C RNA methyltransferase family are METTL2A, METTL2B and METTL8(*17*). METTL2A and METTL2B work on cytosolic $tRNA^{Thr}$ and $tRNA^{Arg}$, respectively. Conversely, METTL8, located in the mitochondria, is responsible for methylation of mitochondrial (mt) $tRNA^{Thr}$ and $tRNA^{Ser}$. All utilize SAM as the source of the methyl group and display remarkable sequence and structure similarity(*17*).

Here, we combine classical and quantum-classical all atom molecular dynamic simulations to elucidate the catalytic mechanism of the methyltransferase reaction promoted by METTL6 and the role of SerRS for tRNA recognition. Importantly, we discover SerRS enhances allosteric signaling between the anticodon stem loop binding site and the N-terminal domain of METTL6, which facilitates correct docking of C_{32} at the METTL6 active site. This propels the methylation reaction, disclosing a mechanism that likely applies to other m^3C methyltransferases.

Results

Seryl-tRNA synthetase impacts tRNA recognition through interaction with the METTL6 N-terminal domain

Cryo-EM structure of the METTL6-SerRS-$tRNA^{Ser}$ complex revealed that SerRS forms a dimeric scaffold able to bind two non-interacting $tRNA^{Ser}$ molecules. Two METTL6 can additionally bind to the complex, one per $tRNA^{Ser}$. However, the cryo-EM structure displaying the highest resolution contained a single METTL6. Therefore, our computer simulations were initiated from this structure (PDBID: 8P7B, Figure 1a)(*11*). The METTL6-SerRS-$tRNA^{Ser}$ complex was resolved in the product state, with the active site containing the already formed m^3C and demethylated SAM, i.e. S-adenosyl-L-homocysteine (SAH) (Figure 1b, c). The latter is held in place by forming hydrogen bonds to I137, R60 and D110 with its amino acid part and

ribose ring. Additionally, the adenosyl moiety is stabilized by forming hydrophobic interactions with F111, L137, T138, A162 and V163. On the other hand, m^3C_{32} is docked in the active site in the so-called flipped-out conformation, pointing away from the anticodon stem loop interior. Its orientation is stabilized by base stacking to F57 and F158. Additionally, R60 forms a hydrogen bond with the C_{32} nucleobase carbonyl group.

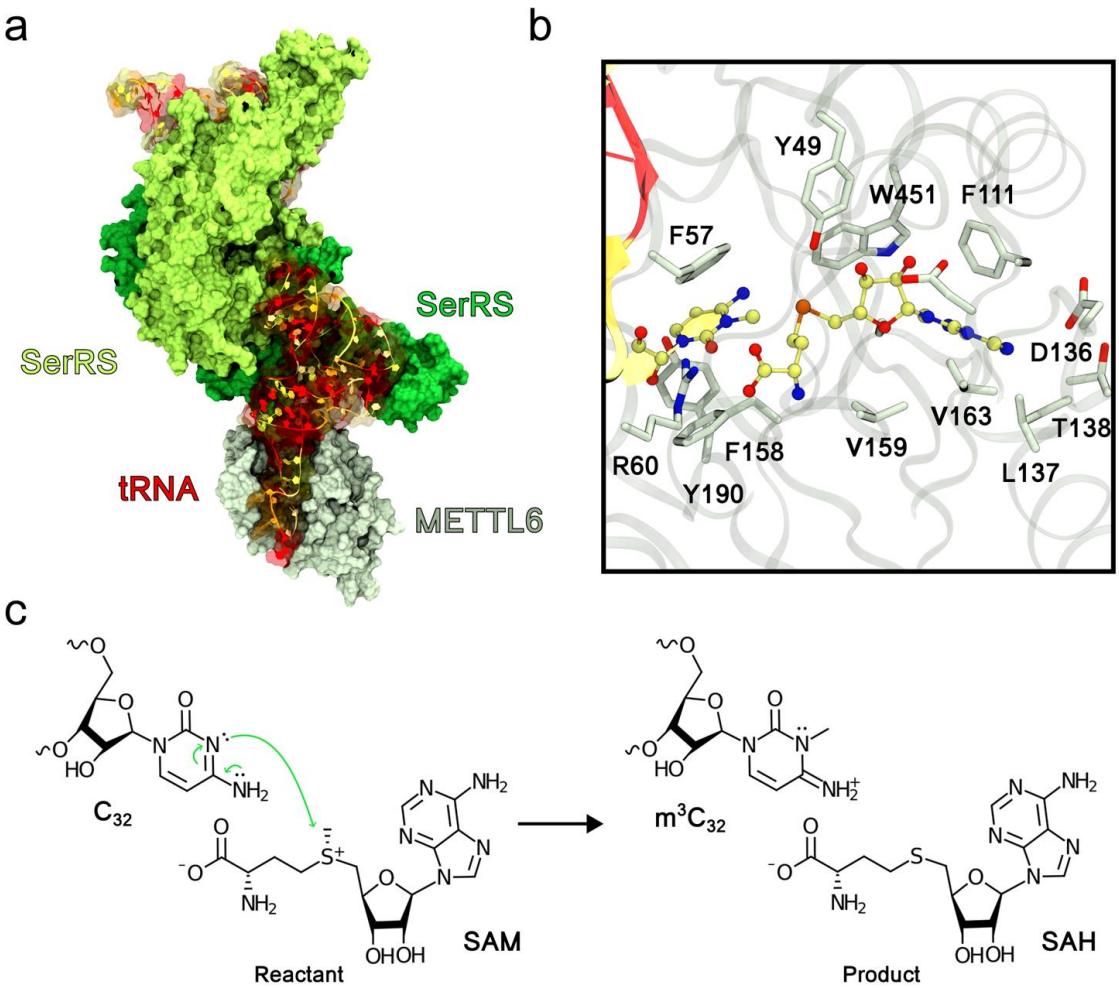

Figure 1. METTL6 is a SAM-based m^3C methyltransferase. (a) Cryo-EM structure of the 1:2:2 METTL6-SerRS-$tRNA^{Ser}$ complex. SerRS and METTL6 are shown as green and white surface, respectively. $tRNA^{Ser}$ is shown with in new ribbons representation. (b) Close up view of the catalytic site of METTL6 as observed in the product state. Residues participating in m^3C_{32} and SAH binding are shown in licorice. (c) Scheme of the methylation reaction. The free electron pair on the N3 atom of C_{32} carries out a nucleophilic attack on the methyl group of

SAM, bound to the positively charged sulfonium cation. This results in the formation of the positively charged m^3C_{32} and neutral SAH.

First, we performed classical MD simulations to assess the role of SerRS for $tRNA^{Ser}$ recognition by METTL6. To recreate the reactant state, where recognition occurs, m^3C_{32} and SAH were converted to C_{32} and SAM. To achieve this, we broke the covalent bond connecting the C_{32}:N3 atom and the methyl group, while reconnecting the latter to the SAH:S atom. We simulated two systems; the full METTL6-SerRS-$tRNA^{Ser}$ complex and the METTL6-$tRNA^{Ser}$ complex in the absence of SerRS. Both systems were described with the CHARMM36m force field(*21*). The complexes were solvated with TIP3P water, and surrounded with KCl ions at 150 mM concentration. Simulations were run in Gromacs for 500 ns in triplicates(*22*).

During classical MD simulations the METTL6-SerRS-$tRNA^{Ser}$ complex remained well-folded, largely maintaining native interfacial contacts between the individual molecular components (Figure 2a-d). Additionally, C_{32} and SAM were stably bound in the active site, with the active site conformation conducive for the methyltransferase reaction for 62 % of simulation time (Figure 2c). To determine which interactions are most important for allosteric communication between $tRNA^{Ser}$ and METTL6, we performed dynamical network analysis using generalized correlations (Figure 2a, b)(*23*). Briefly, based on inter-residue contacts, dynamical network analysis allows us to determine regions of proteins, also called communities, that move in concert and show high degree of correlation. Often these communities correspond or overlap with structural region. Each pair of residues is connected by an edge. The importance of each edge for communication corresponds to its betweenness value, which equals the number of shortest paths between all residue pairs that pass though that edge. Thus, edges characterized with high betweenness values are the most important for communication within the complex. By determining how information is exchanged along the edges, it is possible to identify the dominant communication pathways.

Our analysis revealed that $tRNA^{Ser}$ anticodon stem loop (community 3 in Figure 2b) binding primarily occurs via the internal insertion of METTL6, composed of a short helical run and a β-hairpin (residues 195-220, community 5 in Figure 2b), and the unstructured linker region that follows the N-terminal domain (residues 55-62, community 10 in Figure 2b). Indeed, the relevance of these regions for $tRNA^{Ser}$ recognition was already suggested on the basis of the static cryo-EM structure(*11*). However, while the β-extension region (residues, 246-259, community 6 in Figure 2b) was also singled out as relevant for anticodon stem loop binding by structural analysis, our simulations suggest this region does not play a significant role. Instead,

our simulations indicate that the N-terminal domain (NTD, community 4 in Figure 2b) of METTL6 importantly contributes to anticodon stem loop docking at the active site. However, its influence is exerted indirectly through the tRNA^{Ser} extended variable arm (community 2 in Figure 2b). Specifically, the interaction is predominantly driven by charged residues (Lys43, Asp46, Lys50 and Arg51) hydrogen bonding to the RNA backbone and U47 nucleobase (Figure 2e). This is particularly interesting since SerRS predominantly interacts with METTL6 via NTD.

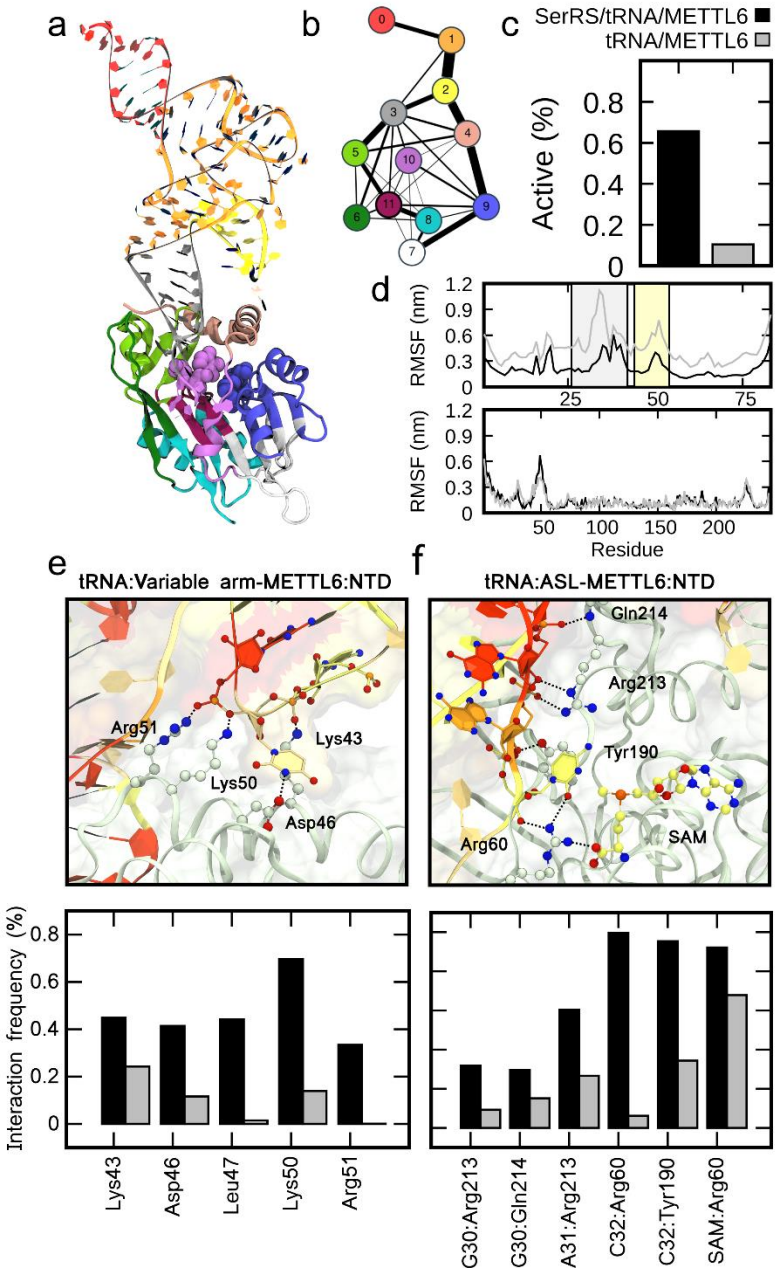

Figure 2. SerRS interactions with METTL6 NTD facilitate tRNA^{Ser} recognition by METTL6. (a) Dynamical network analysis of communication pathways between METTL6 and

$tRNA^{Ser}$ in the full METTL6-SerRS-$tRNA^{Ser}$ complex. Colors indicate different communities. (b) Coarse-grained schematic representation of METTL6-$tRNA^{Ser}$ communication network in presence of SerRS. Circles represent individual communities and edges are depicted with black lines. Edge thickness corresponds to its betweenness value, averaged across all residue pairs between two communities. (c) Probability of a reactive conformation of the active site as observed from classical molecular dynamics. (d) Average residue root mean square fluctuations (RMSF) for $tRNA^{Ser}$ (top panel) and METTL6 (bottom panel). In the top panel the areas shaded in grey and yellow, correspond to the anticodon stem loop and the variable arm, respectively. The black line reports results for the full complex, while the grey line depict results obtained for the METTL6-$tRNA^{Ser}$ complex. (e) Depiction of hydrogen bonding between METTL6 N-terminal domain (NTD) and $tRNA_{Ser}$ variable arm. Bottom panel reports interaction frequencies. Black bars correspond to the full complex, while grey bars show results for the METTL6-$tRNA^{Ser}$ complex. (f) Depiction of hydrogen bonding between METTL6 NTD and $tRNA^{Ser}$ anticodon stem loop (ASL). Bottom panel reports interaction frequencies. Black bars correspond to the full complex, while grey bars show results for the METTL6-$tRNA^{Ser}$ complex.

Strikingly, when simulations were performed in the absence of SerRS, interactions between $tRNA^{Ser}$ variable arm and NTD were significantly disrupted, resulting in complete unbinding of the variable arm from the NTD (Figure 2e). This resulted in increased flexibility of the variable arm that propagated to the anticodon stem loop (Figure 2d). Indeed, interaction between the anticodon stem loop and METTL6 were heavily destabilized, including hydrogen bonds between target C_{32} and Y190 and R60 (Figure 2f). This led to the displacement of C_{32} from the catalytic site and its transition to the flipped-in conformation, with C_{32} engaged in non-canonical base pairing (Figure 2c). Thus, our MD simulations were able to reproduce the experimentally observed importance of SerRS for $tRNA^{Ser}$ binding and methylation by METTL6, suggesting that trimolecular interactions at the METTL6 NTD are of fundamental importance for its activity.

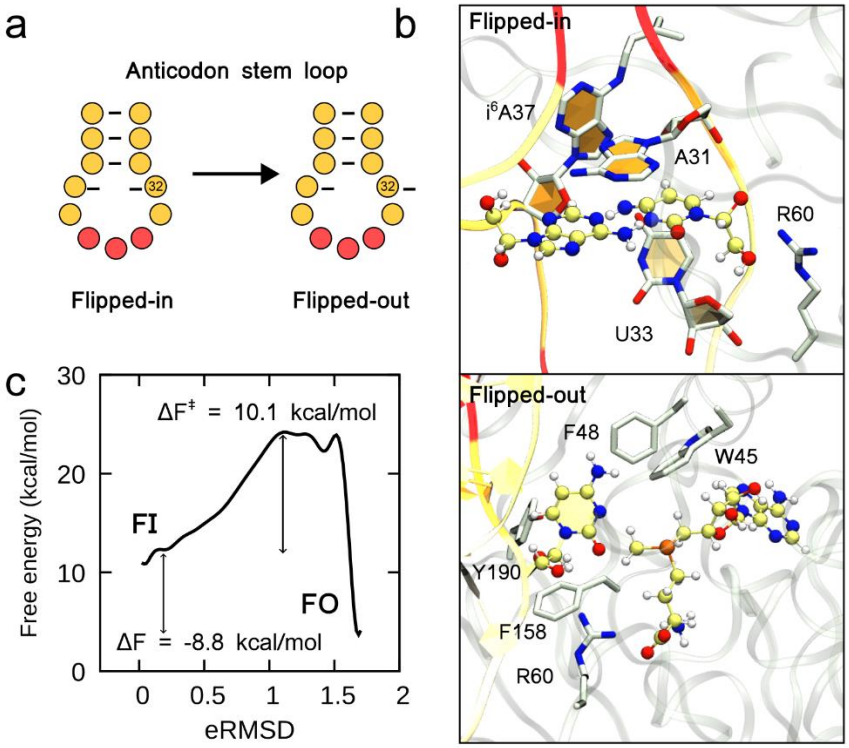

Figure 3. SerRS promotes the tRNA^{Ser} conformational remodelling. (a) Schemes of the flipped-in state observed in free tRNA^{Ser} and the flipped-out state observed in METTL6-SerRS-tRNA^{Ser}. (b) Snapshots of the flipped-in and flipped-out tRNA^{Ser} anticodon stem loop conformations observed during metadynamics simulations. Residues contributing to stabilization of C_{32} in the different tRNA^{Ser} conformational states are shown as licorice. (c) Free energy profile of the tRNA^{Ser} anticodon stem loop conformational transition from the flipped-in to the flipped-out state.

Molecular mechanism of tRNA conformational remodelling

Our MD simulations suggested that SerRS is crucial for correct remodelling of the tRNA^{Ser} anticodon stem loop and for stabilizing the reactive flipped-out conformation of C_{32} (Figure 3a). Conversely, in free tRNA$_{Ser}$ C_{32} is present in a flipped-in conformation, forming a stable non-canonical base pair with A_{38}(*24*). To further investigate the molecular mechanism and energetics of this conformational transition in the full METTL6-SerRS-tRNA^{Ser} complex we performed metadynamics simulations(*25*). As collective variable (CV) we employed eRMSD(*26*) that measures the similarity between two structures by considering only the relative positions and orientations of selected nucleobases (C_{32} and A_{38}). Thus, we were able to sample both the flipped-out and flipped-in conformation (Figure 3b). We determined that in the full complex the flipped-out conformation is more stable in comparison to the flipped-in

conformation by approximately 9 kcal/mol (Figure 3c) This is most likely due to several interactions C_{32} made with the METTL6 residues in the flipped-out conformation. Conversely, in the flipped-in conformation, the C_{32} nucleobase hydrogen bonds to its cognate base, but its orientation is only poorly supported by base stacking to surrounding residues (Figure 3d).

Methyl group transfer is a single-step S_{N2}-like reaction

Finally, we sought to determine the precise molecular mechanism of the methylation reaction. Chemical reactions cannot be simulated with classical MD, since these cannot capture any phenomena involving electron density transfer such as bond breaking and formation(*27*). Instead, hybrid quantum-classical (QM/MM) MD must be employed, where the system is partitioned into two sections; the quantum (QM) zone, covering the active site, and the classical (MM) zone that describes the remainder of the system. This allows for a more accurate treatment of the active site and investigation of reaction mechanisms at an affordable computational cost.

To achieve appropriate sampling, we coupled QM/MM MD simulations with umbrella sampling(*28*). The reaction coordinate (RC) was defined as the difference between the length of the breaking bond (SAM:CH_3-SAM:S) and forming bond (C_{32}:N3-SAM:CH_3) (Figure 4a). Preliminary steered QM/MM MD simulations confirmed this was an appropriate RC for simulating m^3C_{32} formation. The reaction was sampled along 16 windows 0.2 Å apart, spanning the RC range from -1.5 Å to 1.5 Å. Each window was sampled 5-10 ps. Weighted histogram analysis was used to recreate the free energy profile. Methylation of C_{32} to produce m^3C_{32} occurred in a single step. The reaction followed an S_{N2}-like substitution mechanism. The heterocyclic nitrogen atom performed a nucleophilic attack onto the electrophilic methyl group of SAM, activated by the presence of the positively charged sulfonium cation. First, the carbon–sulphur bond was cleaved, followed by formation of the nitrogen–carbon bond (Figure 4a). The transition state (TS) was observed at positive values of RC, indicating a late TS with the leaving group departure more advanced than the nucleophilic attack (Figure 4a-c). Indeed, in TS the methyl group cation is in its unbound state, surrounded by H_2O molecules. The uncharged S-adenosyl-L-homocysteine (SAH) was released as the leaving group, and the resulting methylated nucleoside carried a positive charge, with no m^3C_{32} deprotonation event observed in the product state. The observed activation barrier was approximately 17 kcal/mol, while the reaction free energy was -15 kcal/mol, in line with the extremely favorable energetics (free energy change of −17 kcal/mol) for conversion of SAM to SAH (Figure 4b). Taken together,

our simulations suggest that METTL6 primarily facilitates the methylation reaction by appropriate positioning of reactant species.

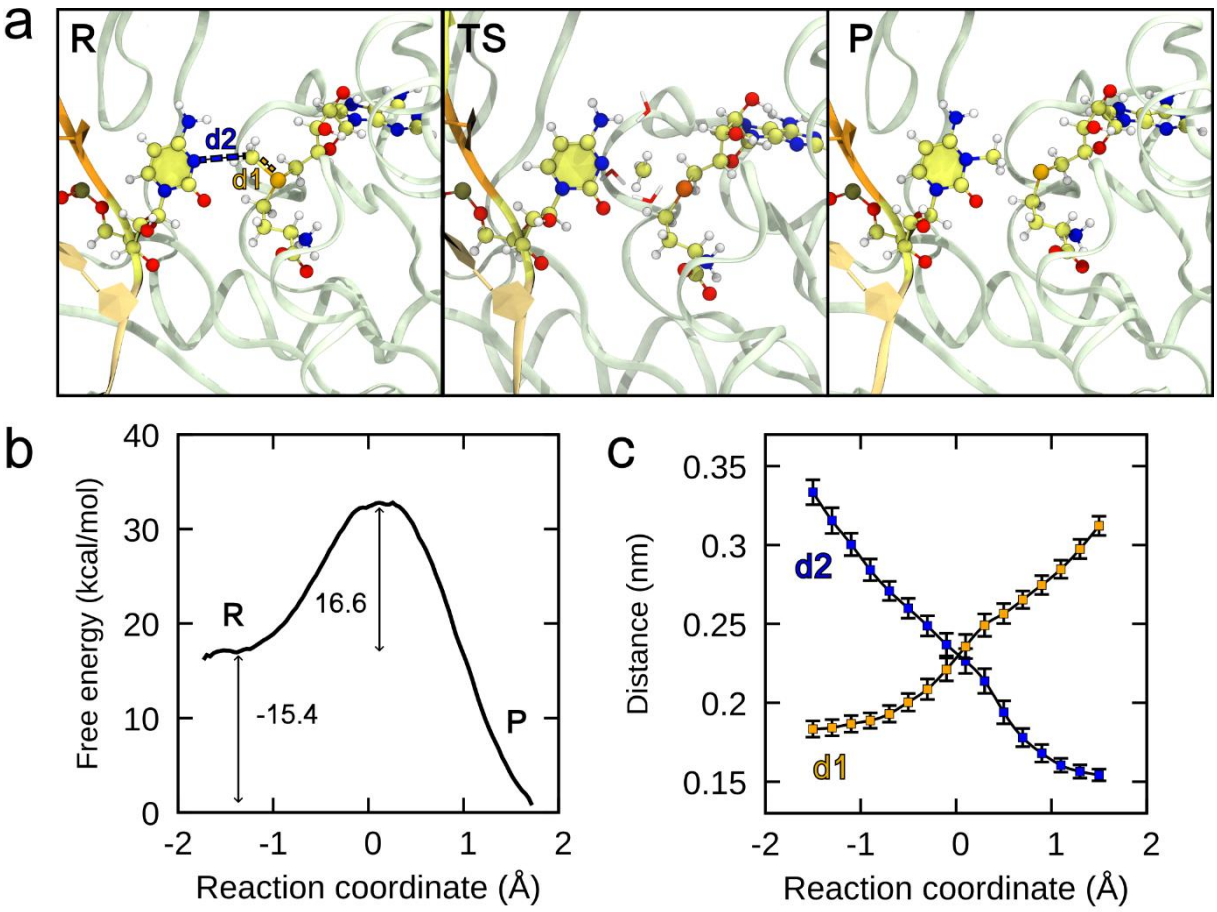

Figure 4. m^{3}C methylation is a concerted S_{N2} reaction. (a) Snapshots of the active site in the reactant (R), transition (TS) and product state (P). Distances used for the definition of the reaction coordinate are shown in orange (d1, SAM:CH_3-SAM:S) and blue (d2, C_{32}:N3-SAM:CH_3). (b) Helmholtz free energy as a function of the reaction coordinate. The reactant (R) and the product state (P) are separated by a single transition state. (c) Values of distances d1 and d2 as defined in panel a as a function of the reaction coordinate.

Discussion

RNA methyltransferases frequently require a protein cofactor to effectively carry out their methylating activity(*3*). These cofactors exhibit diverse mechanisms of methyltransferase activation and can function by promoting binding of the methylating ligand and/or substrate tRNA. Examples of such RNA methyltransferases-protein cofactor complexes outside of m^{3}C methyltransferases include METTL3-METTL14(*36*), where METTL3 is the catalytic domain, METTL1-WDR4(*12*) and FTSJ1-THADA(*37*). While some cofactors function solely as

facilitator of RNA modification, many also have an additional alternative role, like in the case of SerRS. For example, WDR4, that activates METTL1, also aids genome stability by regulating activity of FEN1 endonuclease(*35*). How often aminoacyl-tRNA synthetase are involved in activation of tRNA methyltransferases is unclear and hitherto no other example has been reported in the literature. Interestingly, METTL1 was recently reported to associate with multi-tRNA synthetase complex, promoting tRNA aminoacylation independent of its methylating activity, pointing to a likely two-way aminoacyl-tRNA synthetase-methyltransferase axis(*38*).

Our computer simulations revealed that SerRS promotes METTL6-SerRS-$tRNA^{Ser}$ complex formation and subsequent deposition of m^3C_{32} by stabilizing the $tRNA^{Ser}$ extended variable arm, which leads to onboarding of METTL6 via its NTD. It was previously proposed that SerRS exerts its role through remodeling of the anticodon stem loop. Specifically, it was suggested SerRS stabilizes the flipped-out conformation of C_{32}, exposing it for docking into the METTL6 catalytic cavity as this was observed in structures of many other aminoacyl-tRNA synthetases in complex with their target tRNAs(*29–31*). However, our simulations negate this hypothesis as in the absence of METTL6, SerRS did not disrupt C_{32}:A_{38} non-canonical base pairing. Instead, we propose that anticodon stem loop remodeling is driven by METTL6, once stably docked to $tRNA^{Ser}$. After C_{32} adopts the appropriate conformation in the catalytic site, supported by interaction with Arg60, Tyr190, Phe57 and Phe158, the reaction occurs spontaneously with an activation barrier height characteristic for enzyme catalysis. We posit METTL6 primarily promotes the methylation reaction by organizing the optimal positioning of reactive species, i.e. C_{32} and SAM. The catalytic site of m^3C RNA methyltransferases is highly conserved (Fig. S1) (*17*). Indeed, C_{32} and SAM binding residues are almost identical among human m^3C RNA methyltransferases. This indicates the uncovered catalytic mechanism is likely shared across family members.

Conversely, while NTD sequences of m^3C RNA methyltransferases differ, further indicating NTD is central for tRNA substrate binding specificity, recognition mechanisms of target tRNAs by m^3C RNA methyltransferases likely diverge. Among human m^3C methyltransferases, METTL2A/B requires DALRD3 protein for methylation of $tRNA^{Arg}$(*32*). However, how DALRD3 engages $tRNA^{Arg}$ and METTL2A/B differs from SerRS. Firstly, DALRD3 forms a complex with METTL2A/B in an RNA-independent manner, while SerRS and METTL6 interact only in the presence of $tRNA^{Ser}$. Secondly, the C-terminal domain of DALRD3 is homologous to the anticodon-binding domain of arginyl-tRNA synthetase, suggesting

DALRD3 primarily interacts with the anticodon stem loop of $tRNA^{Arg}$. On the other hand, SerRS does not form contacts with the anticodon stem loop, interacting mainly with the D-arm and the extended variable arm of $tRNA^{Ser}$, absent in the $tRNA^{Arg}$. Taken together, this indicates that the tertiary structure of the METTL2A/B-DALRD3-$tRNA^{Arg}$ complex will significantly variate from METTL6-SerRS-$tRNA^{Ser}$. Indeed, the model complex structure that we predicted with AlphaFold3 gives further credence to this assumption (Fig. S2) (*33*). Furthermore, the N-terminal domain of METTL2A, is in contact with both DALRD3 and the anticodon stem loop, in accordance with the proposed importance of NTD for specific recognition of tRNA substrates. Interestingly, METTL2A/B can modify $tRNA^{Thr}$ independently without a protein cofactor and DALRD3 does not bind to $tRNA^{Thr}$. In contrast, METTL8, that is present in mitochondria, associates with mtSerRS similar to METTL6(*14*, *34*). As SerRS and mtSerRS share a similar fold, it is likely that the METTL8-mtSerRS-$mttRNA^{Ser}$ complex will resemble that of METTL6-SerRS-$tRNA^{Ser}$. Although, the tRNA variable arm may be less crucial for mediating contact between METTL8 and mtSerRS, since $mttRNA^{Ser}$ does not possess an extended variable arm. Indeed, METTL8 and mtSerRS interact also in the absence of tRNA, suggesting a more direct interaction between the protein domains. What is more, METTL8 methylating activity is only modestly increased in the presence of mtSerRS (*14*, *34*).

The apparent specificity of the uncovered SerRS-aided METTL6 recognition mechanism suggests that targeting the METTL6-SerRS-$tRNA^{Ser}$ tertiary interface may lead to the discovery of METTL6-specific therapeutics. In contrast, due to the degeneracy of the active site in m^3C RNA methyltransferases, its targeting could lead to therapeutic compounds with reduced specificity. Yet, due to the interplay of methyltransferases observed in different cancer types, poor selectivity may be beneficial and result in synergistic effects(*18*, *19*, *39*).

In conclusion, our work firmly establishes the catalytic and recognition mechanism of METTL6 in molecular detail, ascertaining the precise role of SerRS and providing concrete indication for viable therapeutic approaches targeting $tRNA^{Ser}$ C_{32} methylation. Future study will further investigate the precise functional role of other RNA modifications in the anticodon stem loop (i^6A_{37}, t^6A_{37}) on C_{32} methylation.

Methods

Classical molecular dynamics (MD)

As the starting point for our molecular dynamics (MD) simulations, we utilized the 1:2:2 METTL6-SerRS-tRNA^{Ser} complex resolved with cryo-EM (PDBID: 8P7B)(*11*). To construct the smaller bimolecular METTL6-tRNA^{Ser} complex, SerRS molecules and the METTL6-unbound tRNA^{Ser} were removed from the complex. System topologies were prepared with CHARMM-GUI web platform(*40*). As forcefields, we employed CHARMM36m that contains parametrizations for all present modified RNA nucleotides(*21*, *41*). Systems were placed in a cubic box and solvated with TIP3P model. KCl salt was added to 150 mM concentration. Classical all-atom MD simulations were performed in GROMACS(*22*). Each simulated system was first equilibrated in the NVT ensemble for 10 ns using periodic boundary conditions and position restraints on the protein and RNA components. Next, equilibration was continued in the NPT ensemble for another 10 ns. Afterwards, position restraints were removed and NPT equilibration was extended for another 10 ns. Newton's equations of motion were solved with the leap-frog algorithm using a 1 fs time step. Electrostatic interactions were evaluated using the particle mesh Ewald method(*42*). Temperature (T) was controlled using the V-rescale thermostat (T = 300 K, coupling constant was 0.1 ps), while pressure will be kept at 1 bar with the Parrinello-Rahman barostat (time constant for pressure coupling was 2 ps)(*43*, *44*). Bonds involving hydrogen atoms were constrained with the LINCS algorithm. For van der Waals interaction, force-switching was applied with 1 nm cutoff. Cutoff for electrostatic and van der Waals interactions was set at 1.2 nm. Production runs were performed in triplicates, each run 500 ns in length, to obtain reliable statistics. Trajectory analysis was performed with Python package MDAnalysis(*45*). Dynamical network analysis was performed with Python package dynetan(*23*). Interactions were analyzed with python package prolif(*46*).

Metadynamics simulations

Conformational remodelling of tRNA^{Ser} anticodon stem loop in the full METTL6-SerRS-tRNA^{Ser} complex was investigated with well-tempered metadynamics(*47*). Metadynamics simulations were performed in GROMACS patched with PLUMED(*26*). As the collective variable we employed eRMSD between nucleotide pair C_{32}:A_{38}. Simulations were performed at 300 K. Bias factor was set at 15 and the tau parameter that determines the rate of Gaussian hill height damping at 70. The width of the Gaussian hills was 0.1 Å. A Gaussian hill was added

to the potential energy surface every 250 steps. Simulations were be performed for 1000 ns. Free energy profile was calculated with the sum_hills utility provided with PLUMED.

Hybrid quantum-classical (QM/MM) molecular dynamics (MD)

QM/MM MD simulations were performed with gromacs utilizing its cp2k interface(*48*). The QM portion was composed of the target nucleotide C_{32}, methyl donor SAM and surrounding water molecules. The quantum box therefore contained 78 atoms. The QM portion was described with the Becke-Lee-Yang-Parr density functional theory (DFT/BLYP)(*49*, *50*). Double-ζ molecularly optimized basis set was used along with Goedecker–Teter–Hutter pseudopotentials (DZVP-MOLOPT-GTH)(*51*). Plane wave cutoff was set at 400 Ry and DFT-D3 dispersion correction was applied(*52*). First, the system was relaxed in the NVT ensemble for 5 ps. MD run parameters equaled those applied during classical MD, however the time step was reduced to 0.5 fs. Following system equilibration, umbrella sampling simulations were performed to obtain the reaction free energy profile(*28*, *53*). We employed a single reaction coordinate (RC), defined as the difference in length of the breaking bond (SAM-C (methyl) – SAM-S) and forming bond (C_{32}-N3 – SAM-C (methyl)). We scanned the RC in the -1.5 Å to 1.5 Å range using a 0.2 Å step size, resulting 16 simulation windows. The harmonic force constant was set at 750 kJ mol^{-1} $Å^{-2}$, to achieve a good overlap between RC distributions of neighboring sampling windows. At each RC value, the system was simulated for 5-10 ps. Free energy profile was reconstructed from pull forces obtained for each simulation window using the weighted histogram analysis method (WHAM) utilizing the gmx wham tool(*54*).

References

1. I. A. Roundtree, M. E. Evans, T. Pan, C. He, Dynamic RNA Modifications in Gene Expression Regulation. *Cell* **169**, 1187–1200 (2017).

2. C. J. T. Lewis, T. Pan, A. Kalsotra, RNA modifications and structures cooperate to guide RNA–protein interactions. *Nat. Rev. Mol. Cell Biol. 2017 183* **18**, 202–210 (2017).

3. C. Höbartner, K. E. Bohnsack, M. T. Bohnsack, How Natural Enzymes and Synthetic Ribozymes Generate Methylated Nucleotides in RNA. *Annu. Rev. Biochem.* **93**, 109–137 (2024).

4. P. C. Dedon, T. J. Begley, Dysfunctional tRNA reprogramming and codon-biased translation in cancer. *Trends Mol. Med.* **28**, 964–978 (2022).

5. N. Manickam, K. Joshi, M. J. Bhatt, P. J. Farabaugh, Effects of tRNA modification on translational accuracy depend on intrinsic codon-anticodon strength. *Nucleic Acids Res.* **44**, 1871–1881 (2015).

6. L. Endres, M. Fasullo, R. Rose, tRNA modification and cancer: Potential for therapeutic prevention and intervention. *Future Med. Chem.* **11**, 885–900 (2019).

7. F. Rapino, S. Delaunay, F. Rambow, Z. Zhou, L. Tharun, P. De Tullio, O. Sin, K. Shostak, S. Schmitz, J. Piepers, B. Ghesquière, L. Karim, B. Charloteaux, D. Jamart, A. Florin, C. Lambert, A. Rorive, G. Jerusalem, E. Leucci, M. Dewaele, M. Vooijs, S. A. Leidel, M. Georges, M. Voz, B. Peers, R. Büttner, J. C. Marine, A. Chariot, P. Close, Codon-specific translation reprogramming promotes resistance to targeted therapy. *Nature* **558**, 605–609 (2018).

8. S. Delaunay, M. Helm, M. Frye, RNA modifications in physiology and disease: towards clinical applications. *Nat. Rev. Genet.* **25**, 104–122 (2024).

9. J. E. Jackman, J. D. Alfonzo, Transfer RNA modifications: nature's combinatorial chemistry playground. *Wiley Interdiscip. Rev. RNA* **4**, 35–48 (2013).

10. W. V. Gilbert, T. A. Bell, C. Schaening, Messenger RNA modifications: Form, distribution, and function. *Science (80-.).* **352**, 1408–1412 (2016).

11. P. Throll, L. G. Dolce, P. Rico-Lastres, K. Arnold, L. Tengo, S. Basu, S. Kaiser, R. Schneider, E. Kowalinski, Structural basis of tRNA recognition by the m3C RNA methyltransferase METTL6 in complex with SerRS seryl-tRNA synthetase. *Nat. Struct.*

Mol. Biol., 1–11 (2024).

12. J. Li, L. Wang, Q. Hahn, R. P. Nowak, T. Viennet, E. A. Orellana, S. S. Roy Burman, H. Yue, M. Hunkeler, P. Fontana, H. Wu, H. Arthanari, E. S. Fischer, R. I. Gregory, Structural basis of regulated m7G tRNA modification by METTL1–WDR4. *Nature* **613**, 391–397 (2023).

13. R. J. Liu, T. Long, J. Li, H. Li, E. D. Wang, Structural basis for substrate binding and catalytic mechanism of a human RNA:m5C methyltransferase NSun6. *Nucleic Acids Res.* **45**, 6684–6697 (2017).

14. M. H. Huang, G. X. Peng, X. L. Mao, J. T. Wang, J. B. Zhou, J. H. Zhang, M. Chen, E. D. Wang, X. L. Zhou, Molecular basis for human mitochondrial tRNA m3C modification by alternatively spliced METTL8. *Nucleic Acids Res.* **50**, 4012–4028 (2022).

15. X.-L. Mao, et al., Mutually exclusive substrate selection strategy by human m3C RNA transferases METTL2A and METTL6. *Nucleic Acids Res.* **49**, 8309–8323 (2021).

16. R. Chen, J. Zhou, L. Liu, X. L. Mao, X. Zhou, W. Xie, Crystal structure of human METTL6, the m3C methyltransferase. *Commun. Biol.* **4**, 1–10 (2021).

17. K. E. Bohnsack, N. Kleiber, N. Lemus-Diaz, M. T. Bohnsack, Roles and dynamics of 3-methylcytidine in cellular RNAs. *Trends Biochem. Sci.* **47**, 596–608 (2022).

18. M. L. Gatza, G. O. Silva, J. S. Parker, C. Fan, C. M. Perou, An integrated genomics approach identifies drivers of proliferation in luminal-subtype human breast cancer. *Nat. Genet.* **46**, 1051–1059 (2014).

19. V. V. Ignatova, S. Kaiser, J. S. Y. Ho, X. Bing, P. Stolz, Y. X. Tan, C. L. Lee, F. P. H. Gay, P. R. Lastres, R. Gerlini, B. Rathkolb, A. Aguilar-Pimentel, A. Sanz-Moreno, T. Klein-Rodewald, J. Calzada-Wack, E. Ibragimov, M. Valenta, S. Lukauskas, A. Pavesi, S. Marschall, S. Leuchtenberger, H. Fuchs, V. Gailus-Durner, M. H. De Angelis, S. Bultmann, O. J. Rando, E. Guccione, S. M. Kellner, R. Schneider, METTL6 is a tRNA m3C methyltransferase that regulates pluripotency and tumor cell growth. *Sci. Adv.* **6**, eaaz4551 (2020).

20. J. Cui, E. Sendinc, Q. Liu, S. Kim, J. Y. Fang, R. I. Gregory, m3C32 tRNA modification controls serine codon-biased mRNA translation, cell cycle, and DNA-damage response. *Nat. Commun.* **15**, 1–14 (2024).

21. J. Huang, S. Rauscher, G. Nawrocki, T. Ran, M. Feig, B. L. De Groot, H. Grubmüller, A. D. MacKerell, CHARMM36m: An improved force field for folded and intrinsically disordered proteins. *Nat. Methods* **14**, 71–73 (2016).

22. M. J. Abraham, T. Murtola, R. Schulz, S. Páll, J. C. Smith, B. Hess, E. Lindahl, GROMACS: High performance molecular simulations through multi-level parallelism from laptops to supercomputers. *SoftwareX* **2**, 1–7 (2015).

23. M. C. R. Melo, R. C. Bernardi, C. De La Fuente-Nunez, Z. Luthey-Schulten, Generalized correlation-based dynamical network analysis: A new high-performance approach for identifying allosteric communications in molecular dynamics trajectories. *J. Chem. Phys.* **153** (2020).

24. P. Auffinger, E. Westhof, Singly and Bifurcated Hydrogen-bonded Base-pairs in tRNA Anticodon Hairpins and Ribozymes. *J. Mol. Biol.* **292**, 467–483 (1999).

25. G. Bussi, A. Laio, Using metadynamics to explore complex free-energy landscapes. *Nat. Rev. Phys.* **2**, 200–212 (2020).

26. G. A. Tribello, M. Bonomi, D. Branduardi, C. Camilloni, G. Bussi, PLUMED 2: New feathers for an old bird. *Comput. Phys. Commun.* **185**, 604–613 (2014).

27. E. Brunk, U. Rothlisberger, Mixed Quantum Mechanical/Molecular Mechanical Molecular Dynamics Simulations of Biological Systems in Ground and Electronically Excited States. *Chem. Rev.* **115**, 6217–6263 (2015).

28. D. Branduardi, F. L. Gervasio, M. Parrinello, From A to B in free energy space. *J. Chem. Phys.* **126** (2007).

29. M. Ruff, S. Krishnaswamy, M. Boeglin, A. Poterszman, A. Mitschler, A. Podjarny, B. Rees, J. C. Thierry, D. Moras, Class II Aminoacyl Transfer Rna Synthetases: Crystal Structure of Yeast Aspartyl-trna Synthetase Complexed with tRNA Asp. *Science (80-.).* **252**, 1682–1689 (1991).

30. B. Delagoutte, D. Moras, J. Cavarelli, tRNA aminoacylation by arginyl-tRNA synthetase: Induced conformations during substrates binding. *EMBO J.* **19**, 5599–5610 (2000).

31. S. I. Sekine, O. Nureki, A. Shimada, D. G. Vassylyev, S. Yokoyama, Structural basis for anticodon recognition by discriminating glutamyl-tRNA synthetase. *Nat. Struct. Biol.* **8**,

203–206 (2001).

32. J. M. Lentini, H. S. Alsaif, E. Faqeih, F. S. Alkuraya, D. Fu, DALRD3 encodes a protein mutated in epileptic encephalopathy that targets arginine tRNAs for 3-methylcytosine modification. *Nat. Commun. 2020 111* **11**, 1–14 (2020).

33. J. Abramson, J. Adler, J. Dunger, R. Evans, T. Green, A. Pritzel, O. Ronneberger, L. Willmore, A. J. Ballard, J. Bambrick, S. W. Bodenstein, D. A. Evans, C. C. Hung, M. O'Neill, D. Reiman, K. Tunyasuvunakool, Z. Wu, A. Žemgulytė, E. Arvaniti, C. Beattie, O. Bertolli, A. Bridgland, A. Cherepanov, M. Congreve, A. I. Cowen-Rivers, A. Cowie, M. Figurnov, F. B. Fuchs, H. Gladman, R. Jain, Y. A. Khan, C. M. R. Low, K. Perlin, A. Potapenko, P. Savy, S. Singh, A. Stecula, A. Thillaisundaram, C. Tong, S. Yakneen, E. D. Zhong, M. Zielinski, A. Žídek, V. Bapst, P. Kohli, M. Jaderberg, D. Hassabis, J. M. Jumper, Accurate structure prediction of biomolecular interactions with AlphaFold 3. *Nature* **630**, 493–500 (2024).

34. N. Kleiber, N. Lemus-Diaz, C. Stiller, M. Heinrichs, M. M. Q. Mai, P. Hackert, R. Richter-Dennerlein, C. Höbartner, K. E. Bohnsack, M. T. Bohnsack, The RNA methyltransferase METTL8 installs m3C32 in mitochondrial tRNAsThr/Ser(UCN) to optimise tRNA structure and mitochondrial translation. *Nat. Commun.* **13**, 1–19 (2022).

35. H. Xu, R. Shi, W. Han, J. Cheng, X. Xu, K. Cheng, L. Wang, B. Tian, L. Zheng, B. Shen, Y. Hua, Y. Zhao, Structural basis of 5′ flap recognition and protein–protein interactions of human flap endonuclease 1. *Nucleic Acids Res.* **46**, 11315–11325 (2018).

36. J. Liu, Y. Yue, D. Han, X. Wang, Y. Fu, L. Zhang, G. Jia, M. Yu, Z. Lu, X. Deng, Q. Dai, W. Chen, C. He, A METTL3-METTL14 complex mediates mammalian nuclear RNA N6-adenosine methylation. *Nat. Chem. Biol.* **10**, 93–95 (2014).

37. K. Ishiguro, A. Fujimura, M. Shirouzu, Structural insights into tRNA recognition of the human FTSJ1-THADA complex. *Commun. Biol.* **8**, 1–11 (2025).

38. R. H. Ali, E. A. Orellana, S. H. Lee, Y. C. Chae, Y. Chen, J. Clauwaert, A. L. Kennedy, A. E. Gutierrez, D. J. Papke, M. Valenzuela, B. Silverman, A. Falzetta, S. B. Ficarro, J. A. Marto, C. D. M. Fletcher, A. Perez-Atayde, T. Alcindor, A. Shimamura, J. R. Prensner, R. I. Gregory, A. Gutierrez, A methyltransferase-independent role for METTL1 in tRNA aminoacylation and oncogenic transformation. *Mol. Cell* **85**, 948-961.e11 (2025).

39. B. W. L. Lee, Y. H. Chuah, J. Yoon, O. V. Grinchuk, Y. Liang, J. L. Hirpara, Y. Shen, L. C. Wang, Y. T. Lim, T. Zhao, R. M. Sobota, T. T. Yeo, A. L. A. Wong, K. Teo, V. D. W. Nga, B. W. Q. Tan, T. Suda, T. B. Toh, S. Pervaiz, Z. Lin, D. S. T. Ong, METTL8 links mt-tRNA m3C modification to the HIF1α/RTK/Akt axis to sustain GBM stemness and tumorigenicity. *Cell Death Dis.* **15**, 338 (2024).

40. E. L. Wu, X. Cheng, S. Jo, H. Rui, K. C. Song, E. M. Dávila-Contreras, Y. Qi, J. Lee, V. Monje-Galvan, R. M. Venable, J. B. Klauda, W. Im, CHARMM-GUI Membrane Builder toward realistic biological membrane simulations. *J. Comput. Chem.* **35**, 1997–2004 (2014).

41. Y. Xu, K. Vanommeslaeghe, A. Aleksandrov, A. D. MacKerell, L. Nilsson, Additive CHARMM force field for naturally occurring modified ribonucleotides. *J. Comput. Chem.* **37**, 896–912 (2016).

42. U. Essmann, L. Perera, M. L. Berkowitz, T. Darden, H. Lee, L. G. Pedersen, A smooth particle mesh Ewald method. *J. Chem. Phys.* **103**, 8577–8593 (1995).

43. G. Bussi, D. Donadio, M. Parrinello, Canonical sampling through velocity rescaling. *J. Chem. Phys.* **126**, 014101 (2007).

44. M. Parrinello, A. Rahman, Polymorphic transitions in single crystals: A new molecular dynamics method. *J. Appl. Phys.* **52**, 7182–7190 (1981).

45. N. Michaud-Agrawal, E. J. Denning, T. B. Woolf, O. Beckstein, MDAnalysis: A toolkit for the analysis of molecular dynamics simulations. *J. Comput. Chem.* **32**, 2319–2327 (2011).

46. C. Bouysset, S. Fiorucci, ProLIF: a library to encode molecular interactions as fingerprints. *J. Cheminform.* **13**, 72 (2021).

47. A. Barducci, G. Bussi, M. Parrinello, Well-tempered metadynamics: A smoothly converging and tunable free-energy method. *Phys. Rev. Lett.* **100**, 020603 (2008).

48. J. Hutter, M. Iannuzzi, F. Schiffmann, J. Vandevondele, Cp2k: Atomistic simulations of condensed matter systems. *Wiley Interdiscip. Rev. Comput. Mol. Sci.* **4**, 15–25 (2014).

49. A. D. Becke, Density-functional exchange-energy approximation with correct asymptotic behavior. *Phys. Rev. A* **38**, 3098–3100 (1988).

50. C. Lee, W. Yang, R. G. Parr, Development of the Colle-Salvetti correlation-energy formula into a functional of the electron density. *Phys. Rev. B* **37**, 785–789 (1988).

51. J. VandeVondele, J. Hutter, Gaussian basis sets for accurate calculations on molecular systems in gas and condensed phases. *J. Chem. Phys.* **127**, 1–10 (2007).

52. S. Grimme, J. Antony, S. Ehrlich, H. Krieg, A consistent and accurate ab initio parametrization of density functional dispersion correction (DFT-D) for the 94 elements H-Pu. *J. Chem. Phys.* **132**, 154104 (2010).

53. G. M. Torrie, J. P. Valleau, Nonphysical sampling distributions in Monte Carlo free-energy estimation: Umbrella sampling. *J. Comput. Phys.* **23**, 187–199 (1977).

54. J. S. Hub, B. L. De Groot, D. Van Der Spoel, G-whams-a free Weighted Histogram Analysis implementation including robust error and autocorrelation estimates. *J. Chem. Theory Comput.* **6**, 3713–3720 (2010).

Acknowledgments

We acknowledge the CINECA award under the ISCRA initiative, for the availability of high performance computing resources and support. J.A. and A.M. thank the PNRR: National Center for Gene Therapy and Drugs based on RNA Technology CUP B83C22002860006 CN_0000004. A.M. is supported by Italian Association for Cancer research (AIRC IG 24514).